Early Period Reanalysis of Ocean Winds and Waves

Andrew T. Cox and Vincent J. Cardone
Oceanweather Inc.
Cos Cob, CT

Val R. Swail
Climate Research Branch, Meteorological Service of Canada
Downsview, Ontario, Canada

1. Introduction

Global reanalysis of ocean winds and waves using atmospheric modeling data produced in the NCEP/NCAR (National Center for Environmental Prediction/ National Centers for Atmospheric Research) and ERA40 (European Centre for Medium-Range Weather Forecasts Reanalysis) projects have proven very successful in determining the wind and wave climate over the past 40-50 years. However, lack of upper air observations prior to the late 1940's makes the production of these products impracticable for the early period of the 20th century using the current methodology. Regional reanalysis projects, such as the AES40 North Atlantic Wind and Wave Climatology (Swail et. al. 2000) made use of these global reanalysis products with the addition of kinematic reanalysis of significant storms using insitu wind observations. This methodology is also limited by the amount of surface data available. Figure 1 shows the distribution of ship reports available in the 1950's (the earliest decade covered by AES40) for a given 6-hour period along with the distribution of the number of COADS observations by year. In periods previous to this date, the distribution of ships lessens to under 1 million per year (globally), which makes it difficult to track the major jet streak features in surface lows.

Statistical methods of extending hindcast datasets such as performed by Wang and Swail (2001) used redundancy analysis to link wind and wave fields to long term known indexes such as the North Atlantic Oscillation (NAO). That study demonstrated that North Atlantic waves in the early 20th century are comparable to those observed in the latter 20th century.

An alternate method of determining the early period wave climate proposed here is to use the daily sea-level pressure data (DSLP) available from the NCAR to derive surface winds and drive a spectral wave model. This paper attempts to make the best possible use of the DSLP analysis archive to explore its use for extending the AES North Atlantic Wind and Wave Hindcast back to 1900. Comparisons of an overlap period of the AES hindcast and DSLP are presented to determine the level of skill in the DSLP hindcast and demonstrate its usefulness in determining the early 20th century period wind and wave climate.

2. Data Sources and Models

2.1 AES40 North Atlantic Wind and Wave Climatology

The AES40 climatology (Swail et. al. 2000) applied a 3rd generation wave model on a .625 by .833 degree latitude-longitude grid

for the 50-year period of June 1955 to June 2004. Wind and wave fields were archived at all grid point locations within the model domain (Figure 2) at a 6-hourly timestep. This hindcast has been extensively validated against insitu and satellite observations and has been found to be very skillful. In this study, the AES40 will serve as the reference dataset for the DSLP derived hindcast fields in order to assess their usefulness.

2.2 Daily Sea Level Pressure Data

The DSLP dataset is a 5-degree once per day field (12 hourly in later periods) of surface pressures mainly derived from historical weather maps. The source data is made available by NCAR as dataset ds101.0 on the DDS data server (dds.ucar.edu). The DSLP data covers the Northern Hemisphere from 15N to the North Pole and extends back in time to January 1899. Figure 3 shows a contoured map from January 1906.

2.3 Presto PBL Model

The Presto (Pressure-to-Wind) marine Planetary Boundary Layer (PBL) model (Cardone 1969) has been applied in numerous hindcast studies including some of the benchmark storms used in wave model development such as SWADE, 1991 "Halloween" storm and 1993 "Storm of the Century" (Cardone et. al. 1995, 1996). On average, a scatter of 3 m/s in wind speed and 30° in wind direction is the intrinsic limit of skill in the specification of synoptic-scale surface winds (Cardone 1991) using this model.

The PBL model was applied to grid point specific gradients of DSLP pressure along with air temperature and air-sea temperature differences. The air and air-sea differences were derived from a database of ship reports stratified by 45-degree directional bins to provide climatological air and air-sea data by wind direction (as determined by the ship wind observation) on a monthly basis.

2.4 UNIWAVE 3rd Generation Wave Model

The 3rd generation UNIWAVE wave model was applied for all DSLP wave hindcasts. The model was identical to the one used in the AES40 climatology (Figure 2). UNIWAVE incorporates deep water and shallow processes and the option to use either OWI's highly calibrated first generation source term physics (ODGP2) or third generation (3G) physics (OWI3G/DIA2). Extensive validations of OWI's wave models in long-term hindcast studies are given recently by Swail and Cox (2000) and Cox and Swail (2001). Details on the 3rd generation physics applied in UNIWAVE can be found in Khandekar *et al*. (1994).

3. Methodology and Comparisons

3.1 Reference Hindcast: 1956

The year 1956 was selected as the benchmark year for DSLP and AES40 hindcasts. It was, at the time, the earliest year of the AES40 hindcast and it was felt that it would be the most representative period of overlap. The 5-degree DSLP pressures were interpolated using a quadratic fitting function to a 2.5-degree field for input to the PBL model. The output of the PBL model gave once-per-day 10-meter wind fields valid at 12 GMT each day. Since the DSLP data only extended to 15N, the rest of the AES40 wave model domain (0N to 15N) was filled using long-term monthly winds derived from the NCEP/NCAR reanalysis. The 15-20N regions were treated as a blending zone to minimize discontinuities between the fields.

Simple linear interpolation of the once-per-day wind fields in time would result in smearing of the major wind features, so a moving centers interpolation algorithm was applied. Pressure fields from the DSLP were brought into the Wind WorkStation (WWS, Cox et al. 1995) and the major low-pressure systems were identified and tracked from day to day. The moving centers algorithm preserves the bearing/range of winds with respect to each center within a determined radius of influence. Winds outside the moving center are subject to normal linear interpolation. Figure 4 shows the difference between linear interpolation (top) and moving centers interpolation (bottom) for a low-pressure system tracked on January 1st 1906.

The time-interpolated wind fields were then put on the AES40 wave grid (.625 by .833 degree) and run through the UNIWAVE model. Figures 5 and 6 show the mean significant wave height pattern by season for the DSLP and AES40 hindcasts. While the general pattern of the wave heights is similar between the hindcasts there is a significant bias low of the DSLP results. This bias can be directly attributed to the wind fields that also show a systematic bias when compared to the AES40 winds. The overall energy level is too low primarily due the coarse time resolution (daily) of the source DSLP data. A comparison of the 1990 DSLP derived winds, which are available twice per day, shows that such a bias between the AES40 6-hourly and DSLP interpolated 6-hourly winds is significantly reduced.

In order to reduce the bias in the DSLP derived waves a distributional comparison of the winds from each hindcast was performed to produce a general correction factor that could be applied to the DSLP winds. All matching grid points for the entire year were used to produce one quantile-quantile comparison. Season differences (Figure 7) and regional differences (Figure 8) were also explored to determine if such a stratified approach was justified. The season differences (Figure 7) show very little change from the full year comparison. In the selected points, the regions of maximum DSLP/AES40 differences were plotted to see just how far off the correction factor could be. Figure 8 shows that even in the most biased regions the correction factor improves the DSLP winds and the quantile differences are within 2 m/s.

The adjusted DSLP winds were run through the UNIWAVE model and comparisons against the AES40 mean waves by season are shown in Figures 9 and 10. General features are very similar in the hindcasts. Largest differences occur in the areas of maximum mean wave height, particularly in the fall (Oct-Nov-Dec).

The mean difference in the wave heights (DSLP-AES40, Figure 11) shows that the DSLP hindcast is now biased slightly high (12 cm overall, Table 1), but the vast majority of the area the bias is under 10 cm with some maximum difference areas of 20 cm. A quantile-quantile comparison (Figure 12) shows that there is near linear agreement of the two hindcasts up to the 99th percentile. Interesting, the wave results do show more deviations in the seasons than is indicated by the source winds. The spring-summer period accounts for the majority of the over-estimation while the fall-winter period is much closer to the 45-degree line.

Table 1 Wind and wave statistics for comparison of AES40 and DSLP hindcasts for 1956. (Mean difference (DSLP- AES40), standard deviation, scatter index and correlation coefficient)

Variable	Diff (DSLP-AES40	Std Dev.	SI	CC
Ws (m/s)	-.25	2.19	28%	82%
Hs (m)	.12	.62	26%	91%

3.2 Comparison Hindcasts: 1990 and 1906

Two different years, both associated with strongly positive values of the NAO index (2.29 for 1906 and 3.88 for 1990), were selected for hindcast with the DSLP data. The year 1990 will serve as a test of the validity of the DSLP methodology while the year 1906 was chosen simply for its positive NAO index.

Hindcast methodology for the two years remained the same, new files of moving centers were generated for each and the same wind adjustments applied. The 1990 data contained twice-per-day fields at 00 and 12 GMT. In order to preserve the methodology and produce a validation set consistent with the early period data (once per day) the 00 GMT pressure fields were discarded. Table 2 shows the overall statistical comparison of the DSLP and AES40 hindcasts for 1990. The mean differences and associated statistics are very similar to the 1956 reference case, suggesting the wind modifications are valid independent of year. However, Figure 13 shows that there are larger coherent regions of over and under estimation. The seasonal quantile-quantile comparison (Figure 14) shows the overestimation in the full year results and in the seasons. As in the 1956 case, the 1990 comparisons are very linear up to the 99th percentile and the stormier fall/winter period shows better agreement than the spring/summer period.

Table 2 Wind and wave statistics for comparison of AES40 and DSLP hindcasts for 1990. (Mean difference (DSLP-AES40, standard deviation, scatter index and correlation coefficient)

Variable	Diff (DSLP-AES40	Std Dev.	SI	CC
Ws (m/s)	-.20	2.21	28%	84%
Hs (m)	.21	.63	26%	92%

Figures 15 and 16 show the mean significant wave height by season for both 1906 and 1990. Patterns from each show strong waves, particularly in the January-February-March period. The 1990-year, associated with a very high value of the NAO, shows stronger waves overall but both NAO years show similar patterns as to the placement of the wave maxima.

4. Conclusions

In this study, a methodology was explored to make use of the Daily Sea Level Pressure (DSLP) dataset of 5-degree Northern Hemisphere surface pressure data for extension of wind and wave climatology back to the year 1900. A comparison with the AES40 hindcast during an overlap period (year of 1956) suggested a wind adjustment factor be applied to increase the overall energy level of the DSLP derived winds. This adjustment is linked to the temporal resolution of the DSLP early period data of once per day fields. This adjusted hindcast was then compared to an independent year of the AES40 (1990) and found to be quite skillful with a mean wind bias of -.20 m/s and wave bias of .21 m with scatter indexes of 28% and 26% respectively.

In conclusion, the methodology based on two reference years in different decades suggests that the DSLP data can be applied for early period reanalysis. Future work should include a larger overlap period of

AES40 for comparison and investigation of seasonal differences in DSLP waves.

References

Cardone, V. J., 1969. Specification of the wind field distribution in the marine boundary layer for wave forecasting . Report TR-69-1, Geophys. Sci. Lab.. Available from NTIS AD# 702-490.

Cardone, V.J. 1991. The LEWEX wind fields and baseline hindcast. Directional Ocean Wave Spectra, R.C. Beal Ed., The Johns Hopkins University Press, 136-146.

Cardone, V. J., R. E. Jensen, D. T. Resio, V. R. Swail and A. T. Cox. Evaluation of contemporary ocean wave models in rare extreme events: Halloween storm of October, 1991; Storm of the century of March, 1993**.** J. of Atmos. And Ocean. Tech., 13, 198-230.

Cardone, V. J., H. C. Graber, R. E. Jensen, S. Hasselmann, M. J. Caruso 1995. In search of the true surface wind field in SWADE IOP-1: Ocean wave modelling perspective. The Global Atmosphere and Ocean System, 3, 107-150.

Cox, A.T., J.A. Greenwood, V.J. Cardone and V.R. Swail. An Interactive Objective Kinematic Analysis System Fourth International Workshop on Wave Hindcasting and Forecasting. October 16-20, 1995. Banff, Alberta, Canada.

Cox, A.T. and V.R. Swail. A Global Wave Hindcast over the Period 1958-1997: Validation and Climate Assessment. JGR (Oceans), Vol. 106, No. C2, pp. 2313-2329, February 2001.

Khandekar, M. L., R. Lalbeharry and V. J. Cardone. 1994. The performance of the Canadian spectral ocean wave model (CSOWM) during the Grand Banks ERS-1 SAR wave spectra validation experiment. Atmosphere-Oceans, 32, 31-60.

Swail, V.R., E.A. Ceccacci and A.T. Cox. The AES40 North Atlantic Wave Reanalysis: Validation and Climate Assessment. 6th International Workshop On Wave Hindcasting and Forecasting, November 6-10, 2000 Monterey, California, USA.

Wang, X.L. and V.R. Swail. Changes of Extreme Wave Heights in Northern Hemisphere Oceans and Atmospheric Circulation Regimes. Journal of Climate, vol 14, pp2204-2221, 2001.

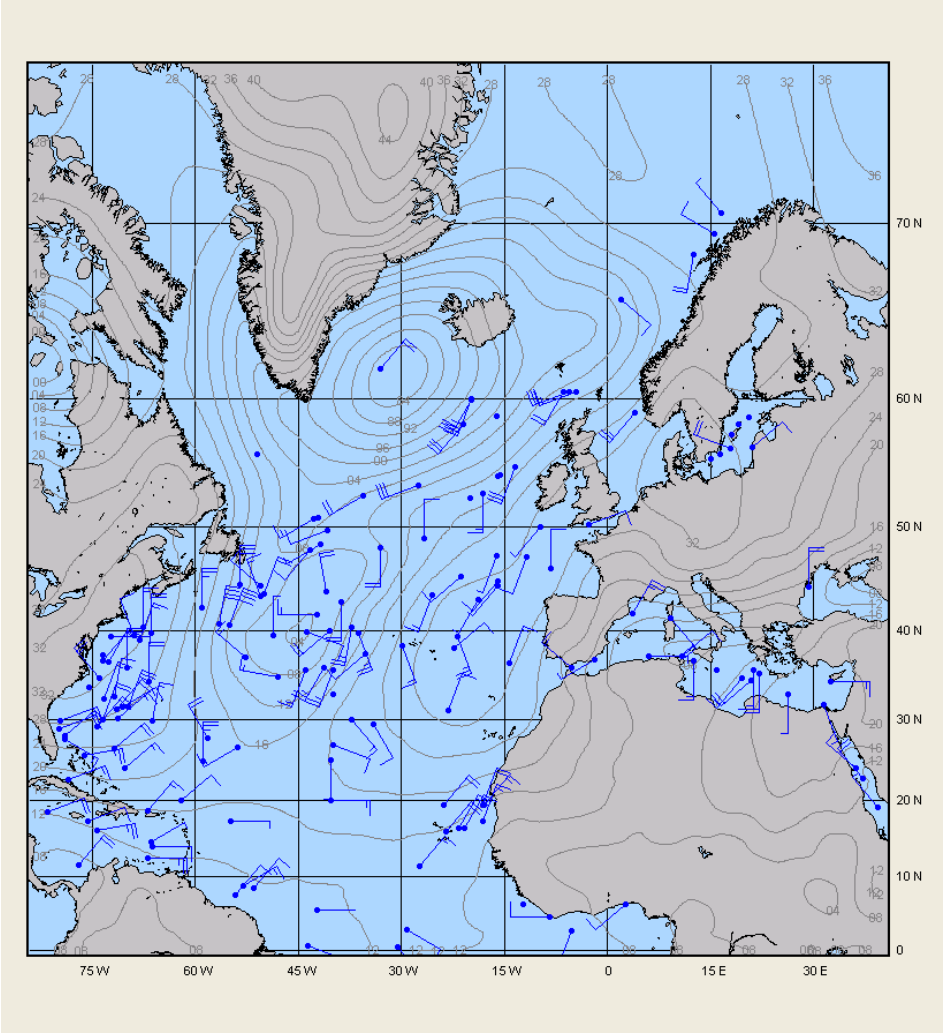

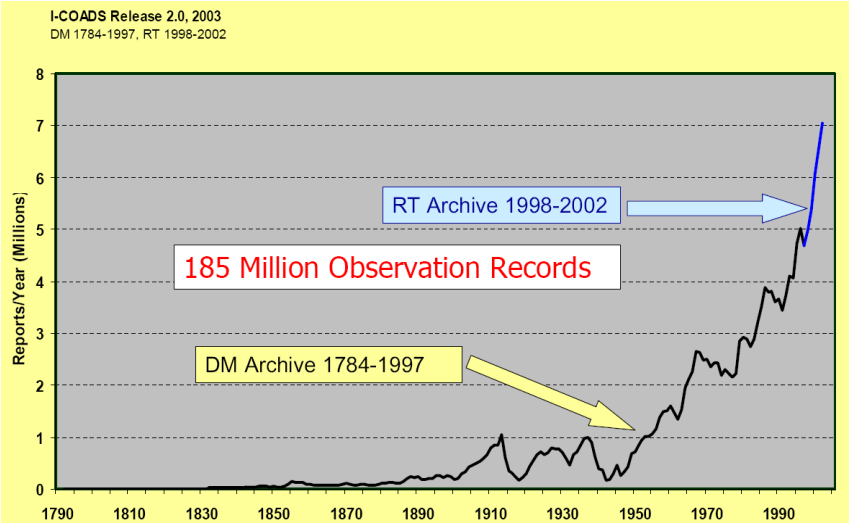

Figure 1 Ship reports from January 1 1950 with NCEP/NCAR Reanalysis pressure (mb) contours (above) total globally available COADS observations by year (below)

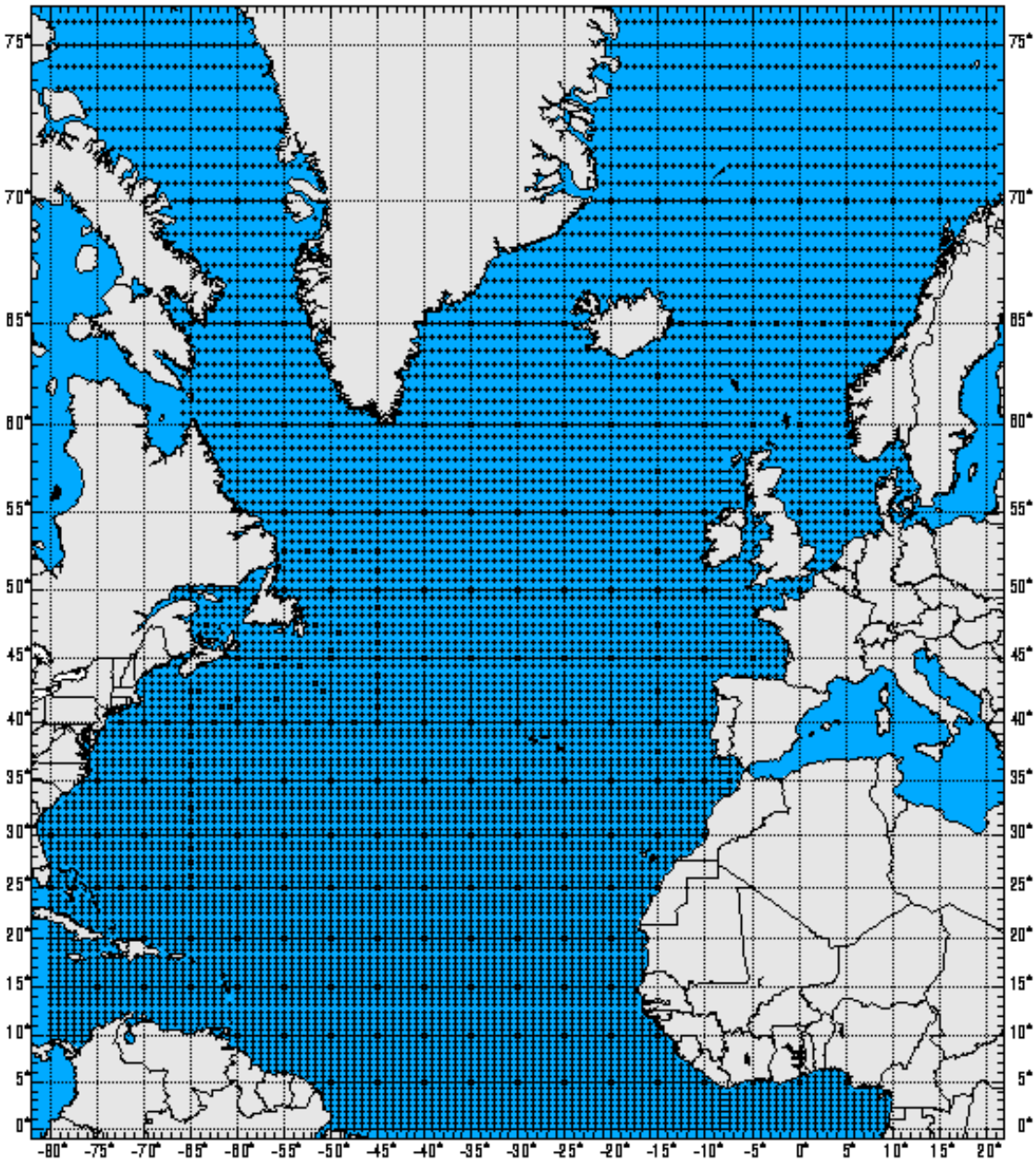

Figure 2 AES40 wind and wave domain

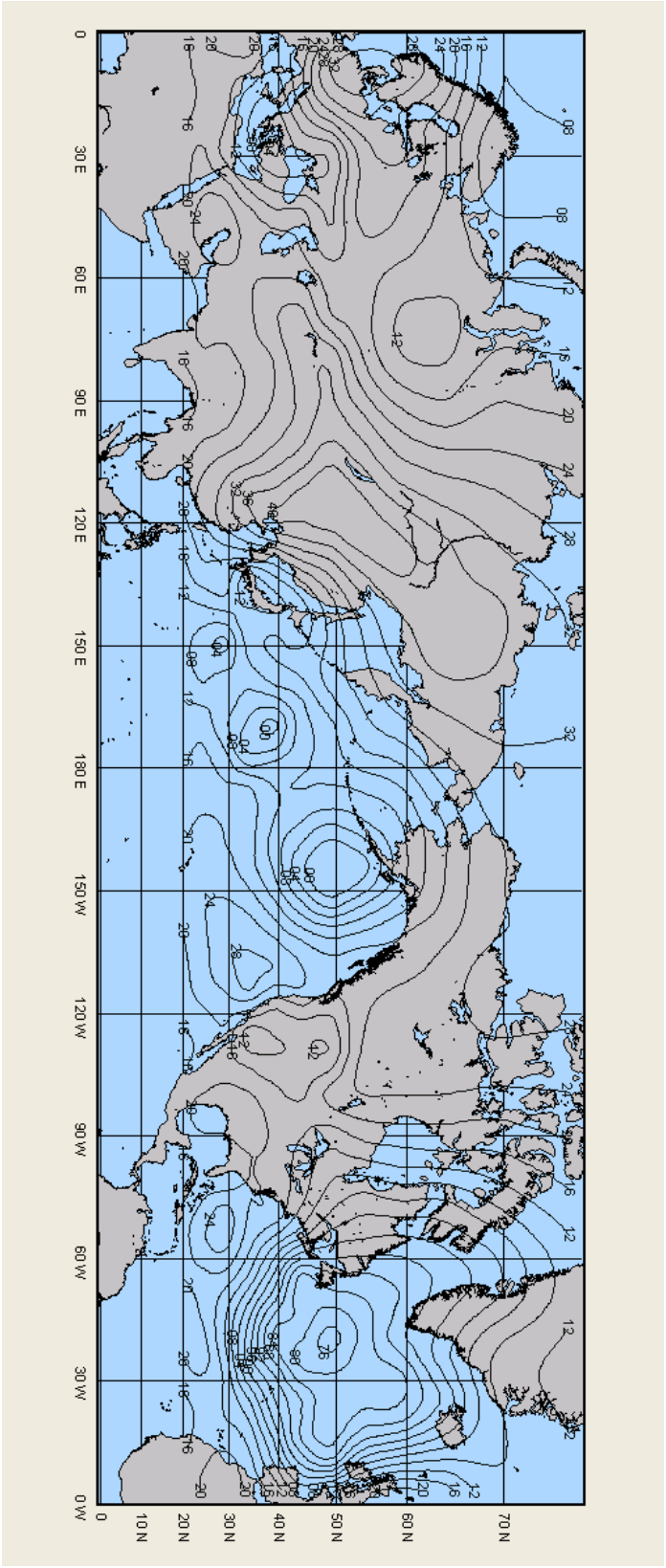

Figure 3 DSLP pressure contours for January 01 1906 12 GMT

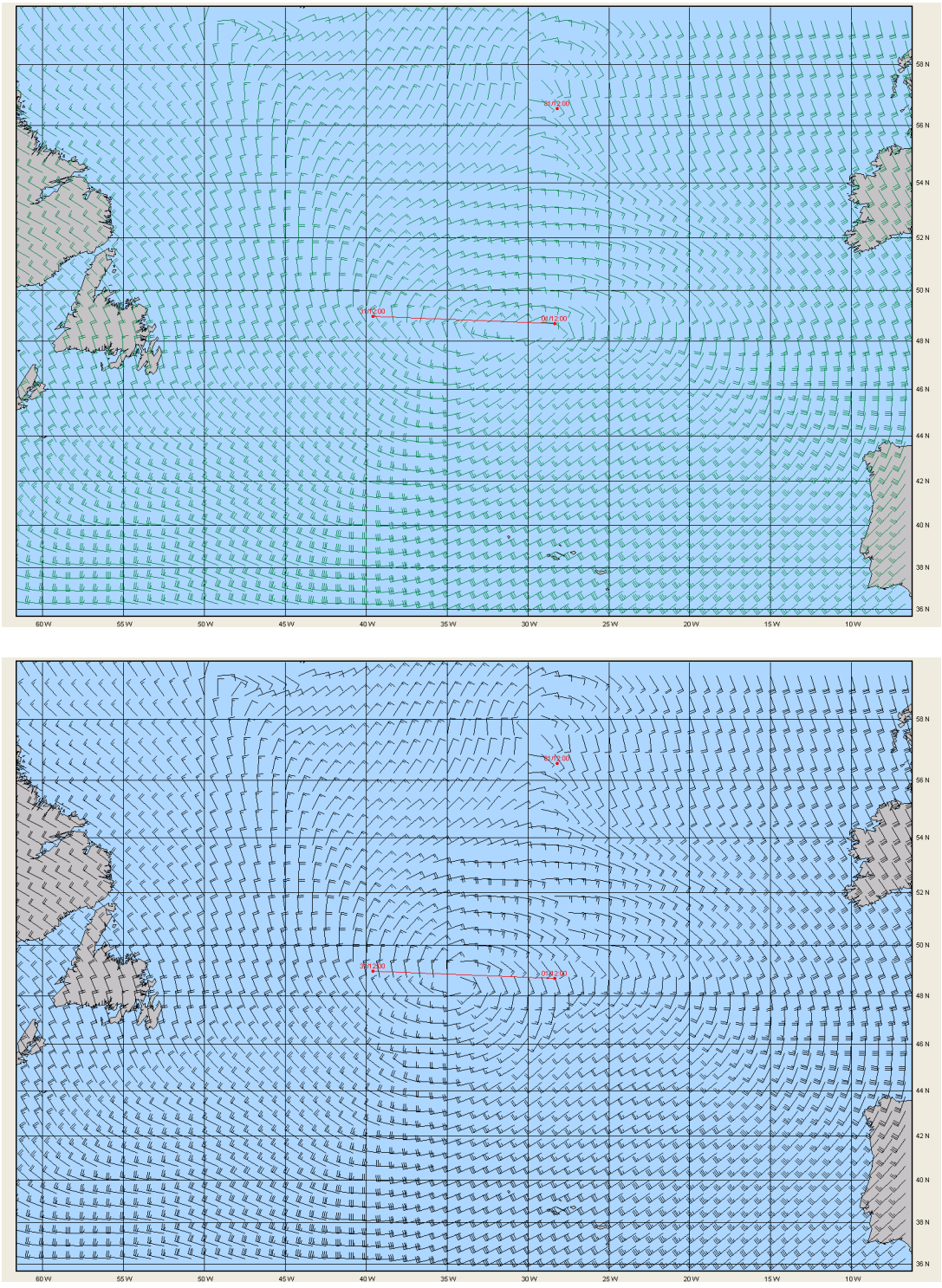

Figure 4 Time interpolated winds for Jan 01 1906 00 GMT using linear interpolation (top) and moving centers interpolation (bottom). Position of the low pressure center is indicated by red circles +/- 12 hours.

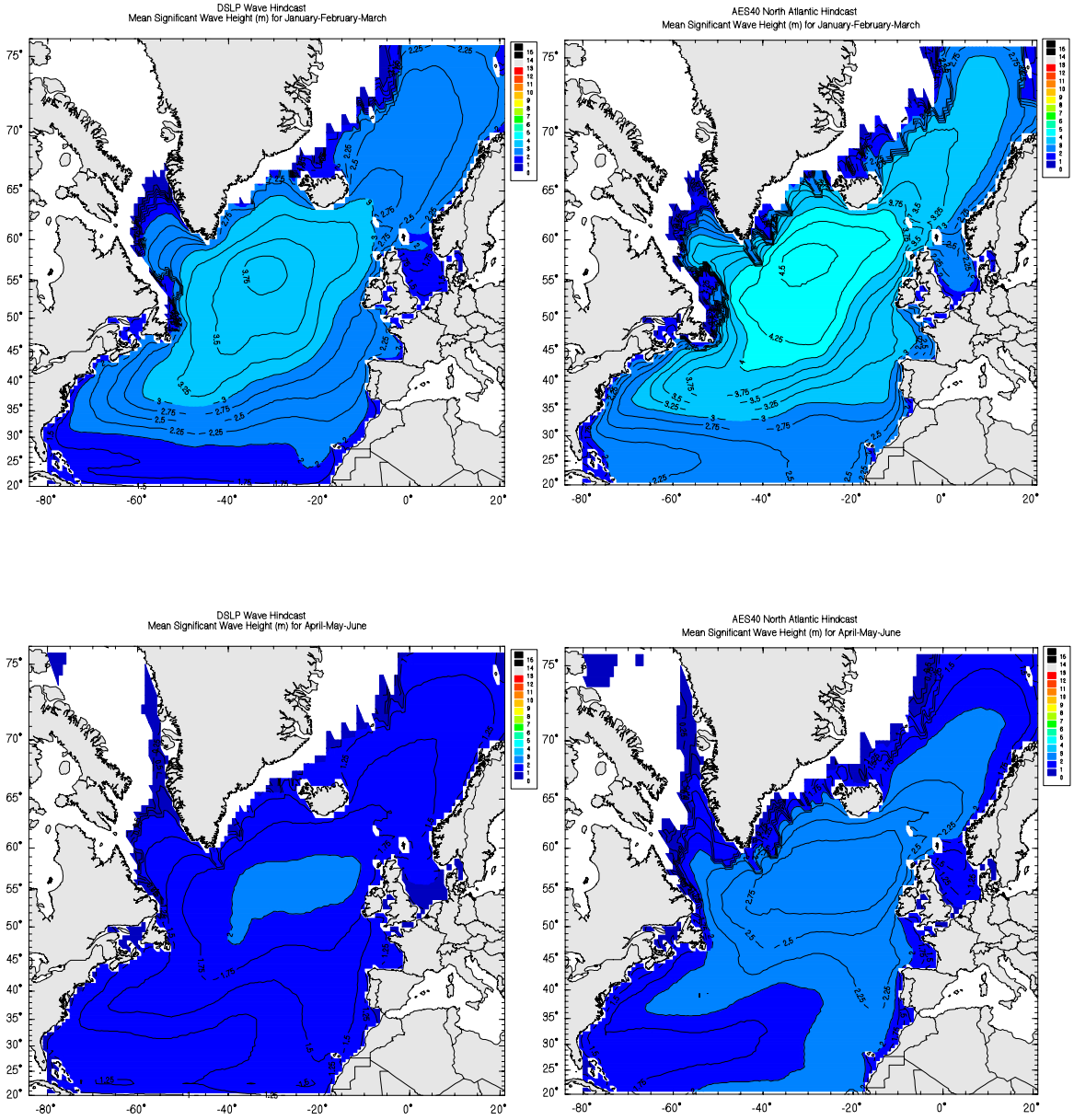

Figure 5 Dec-Jan-Feb 1956 (top) and Apr-May-Jun 1956 (bottom) mean significant wave height for DSLP (left) and AES40 (right) hindcast

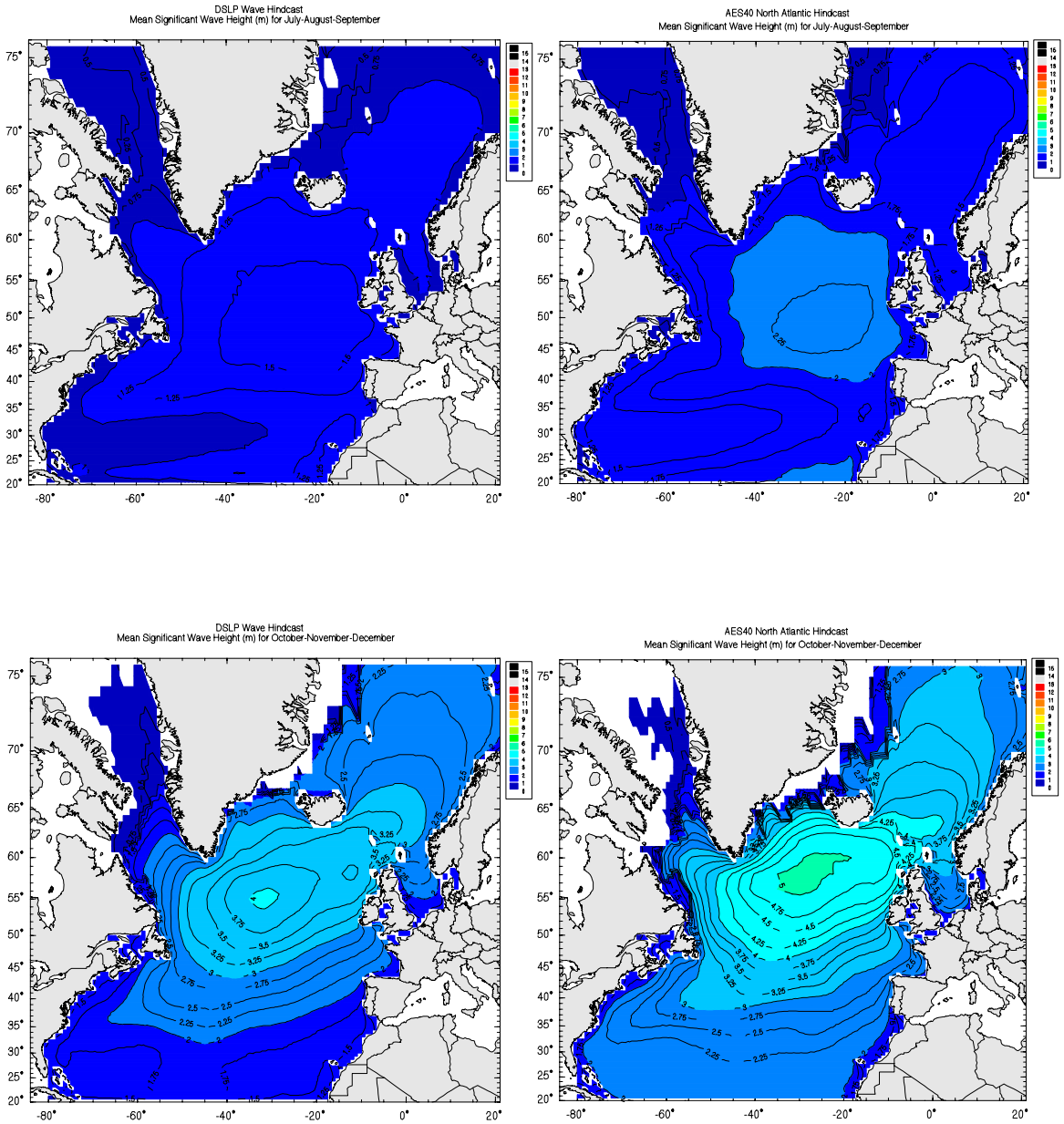

Figure 6 Jul-Aug-Sep 1956 (top) and Oct-Nov-Dec 1956 (bottom) mean significant wave height for DSLP (left) and AES40 (right) hindcast

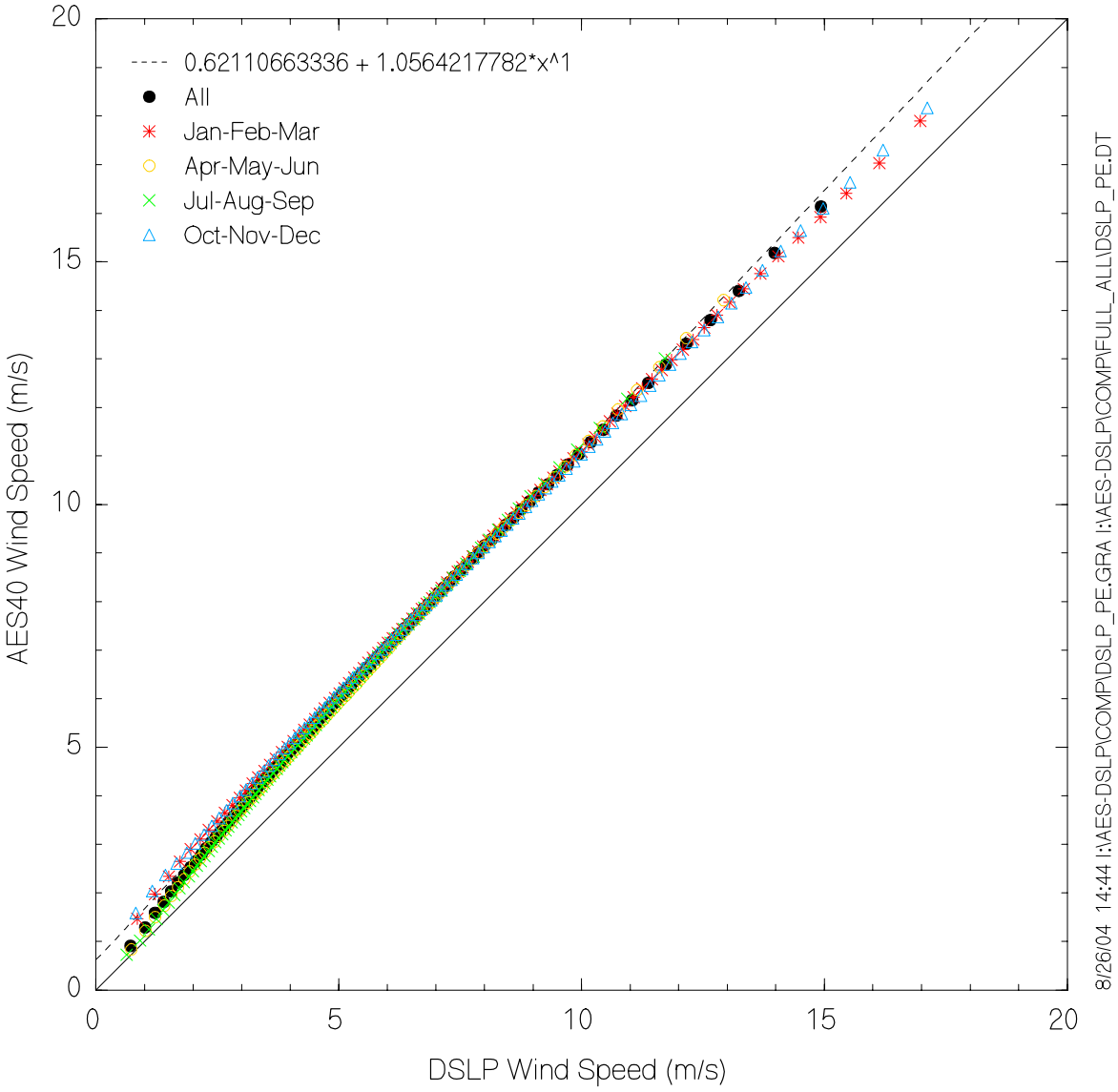

Figure 7 Quantile-quantile comparisons of DSLP and AES40 wind speeds in 1956 by season

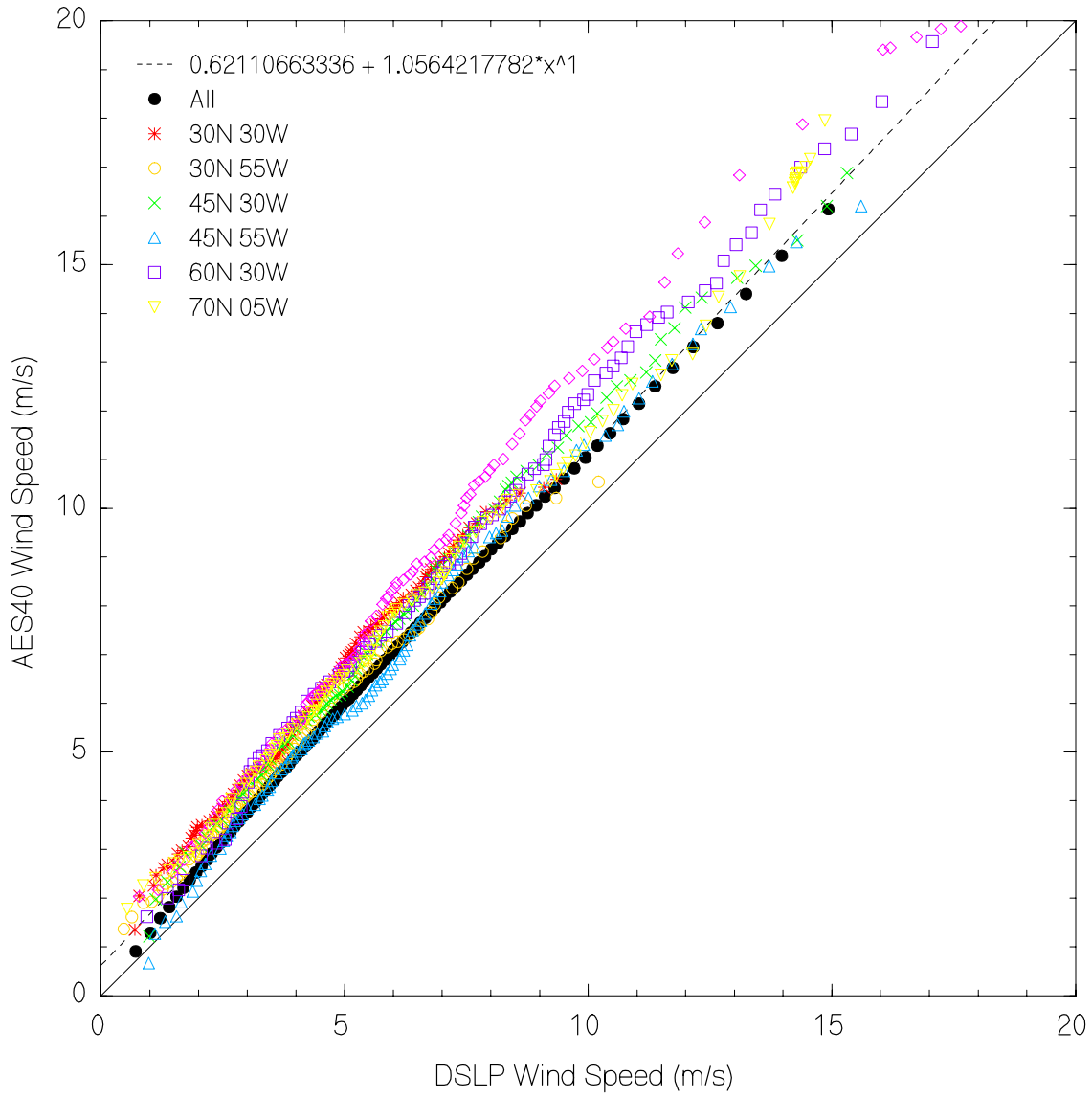

Figure 8 Quantile-quantile comparisons of DSLP and AES40 wind speeds in 1956 for selected locations

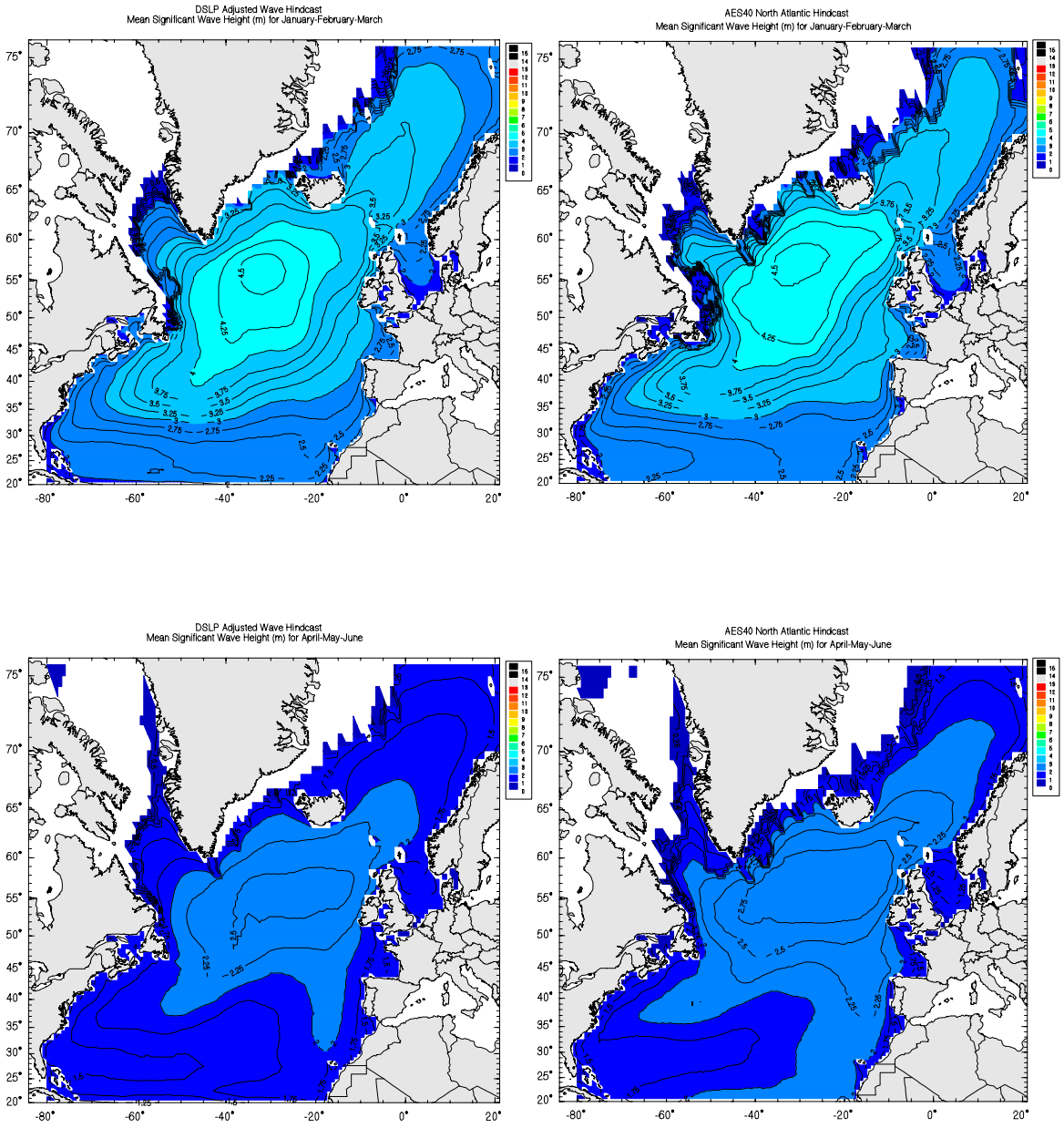

Figure 9 Dec-Jan-Feb 1956 (top) and Apr-May-Jun 1956 (bottom) mean significant wave height for DSLP Adjusted (left) and AES40 (right) hindcast

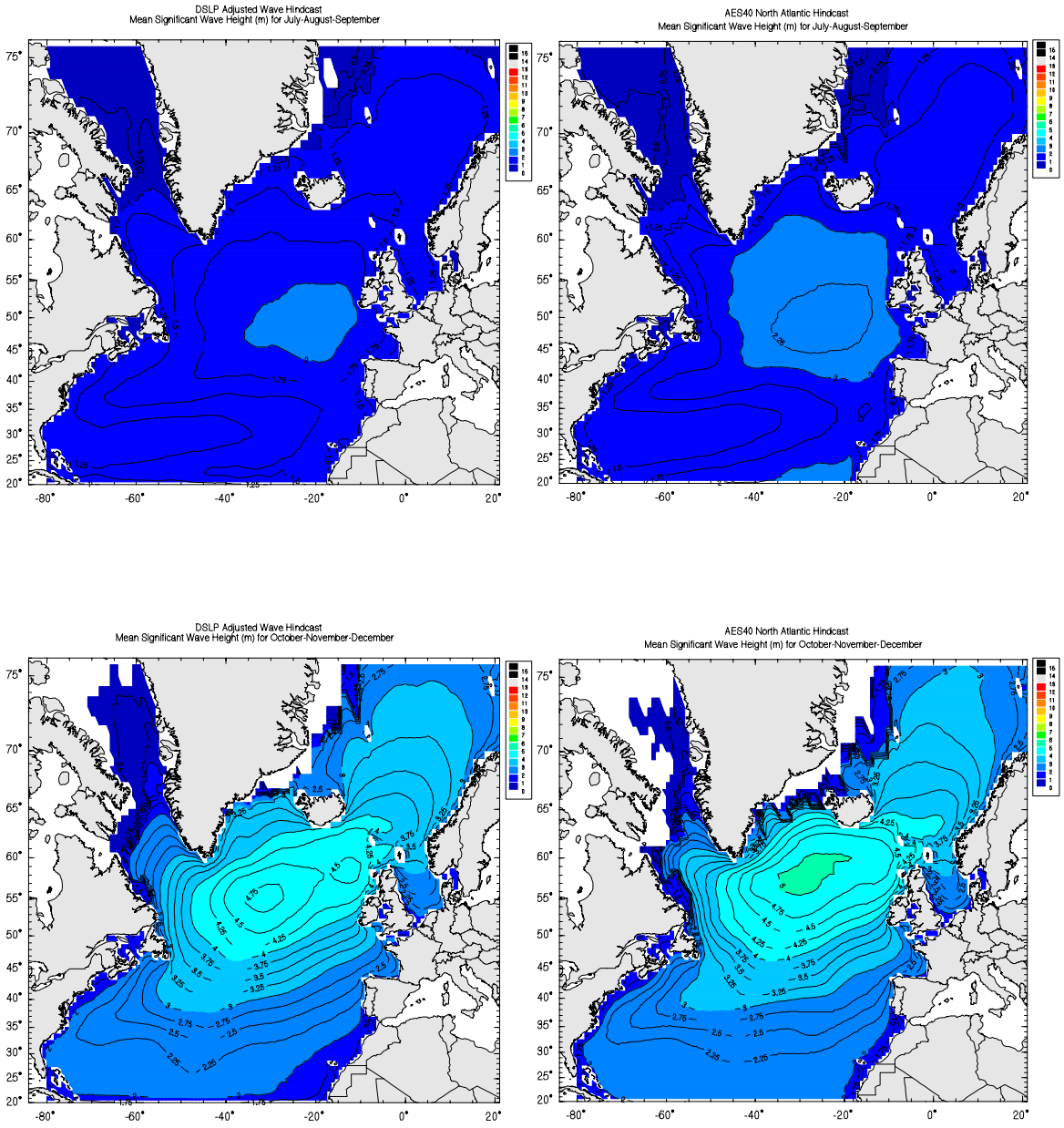

Figure 10 Jul-Aug-Sep 1956 (top) and Oct-Nov-Dec 1956 (bottom) mean significant wave height for DSLP Adjusted (left) and AES40 (right) hindcast

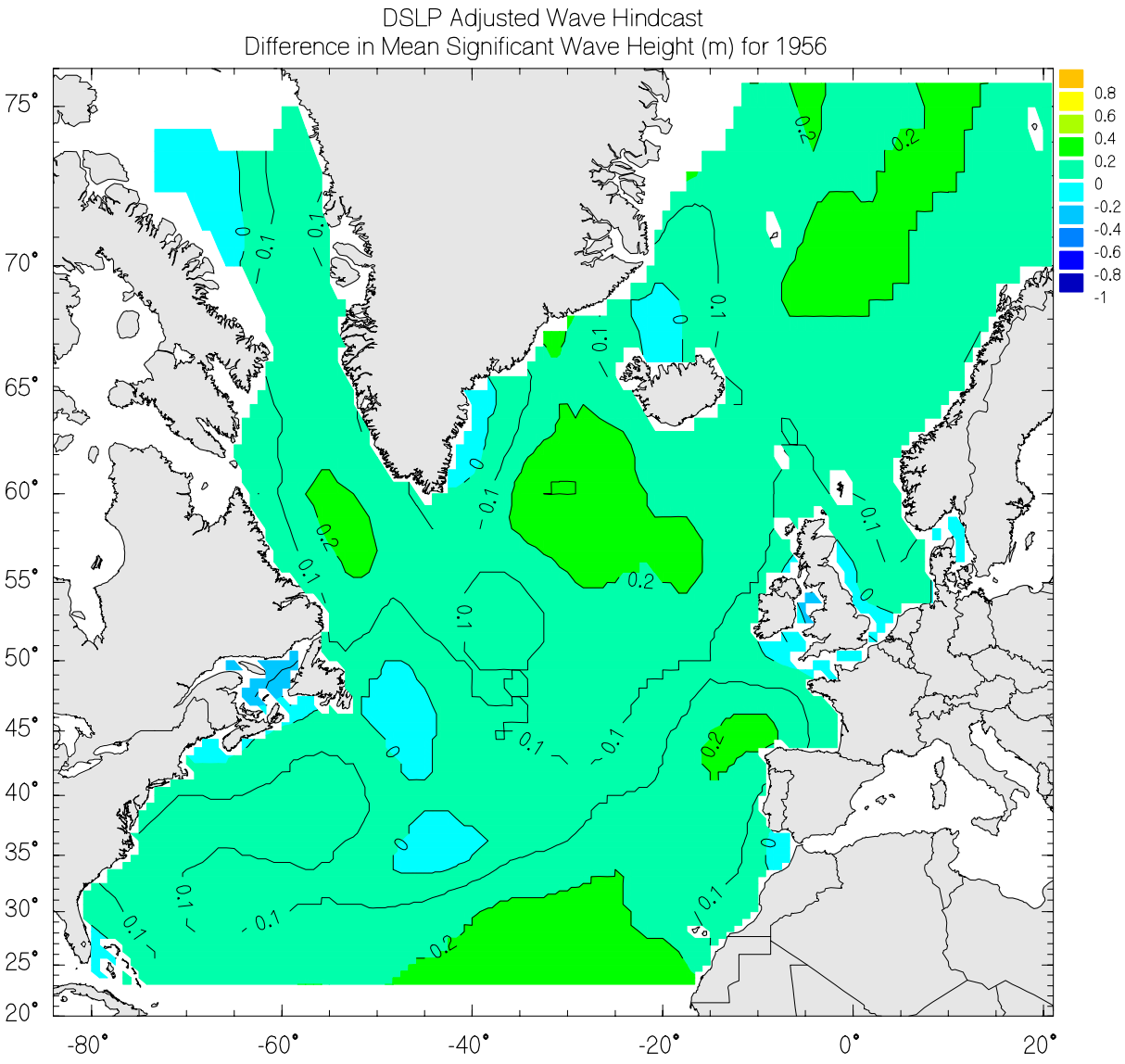

Figure 11 Difference in mean significant wave height (DSLP-AES40) for 1956

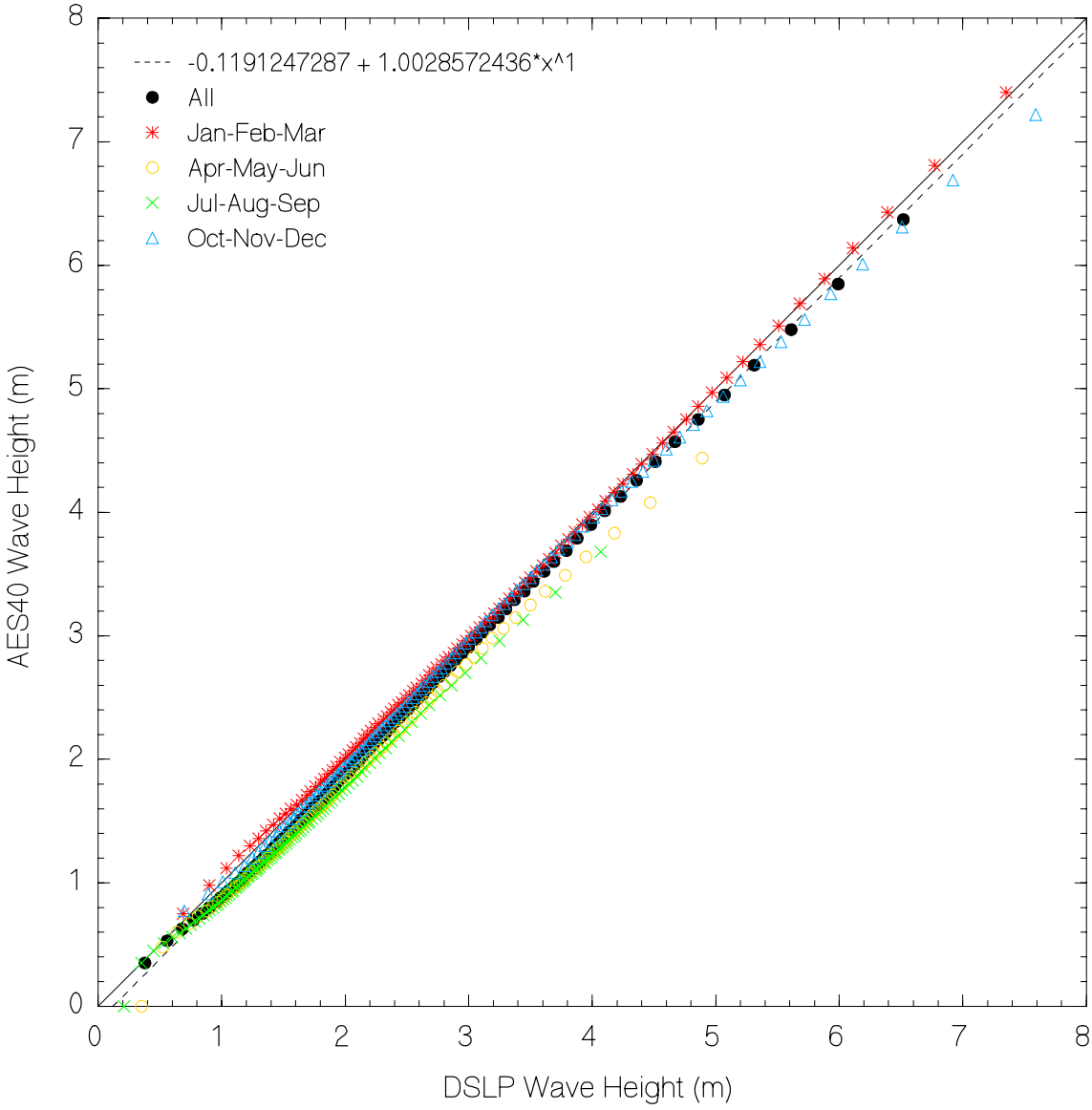

Figure 12 Quantile-quantile comparisons of DSLP (adjusted) and AES40 wave height (m) in 1956 by season

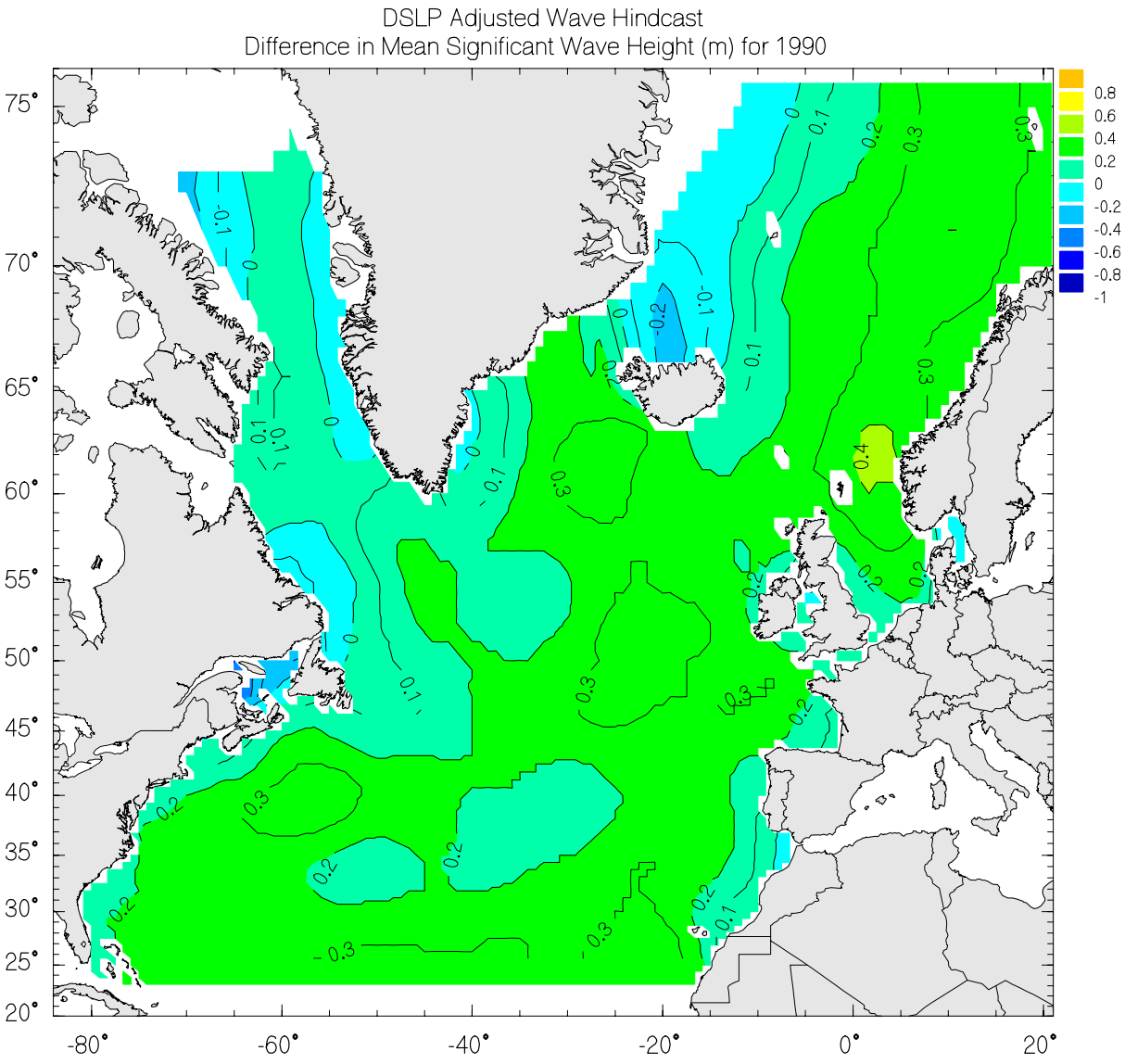

Figure 13 Difference in mean significant wave height (DSLP-AES40) for 1990

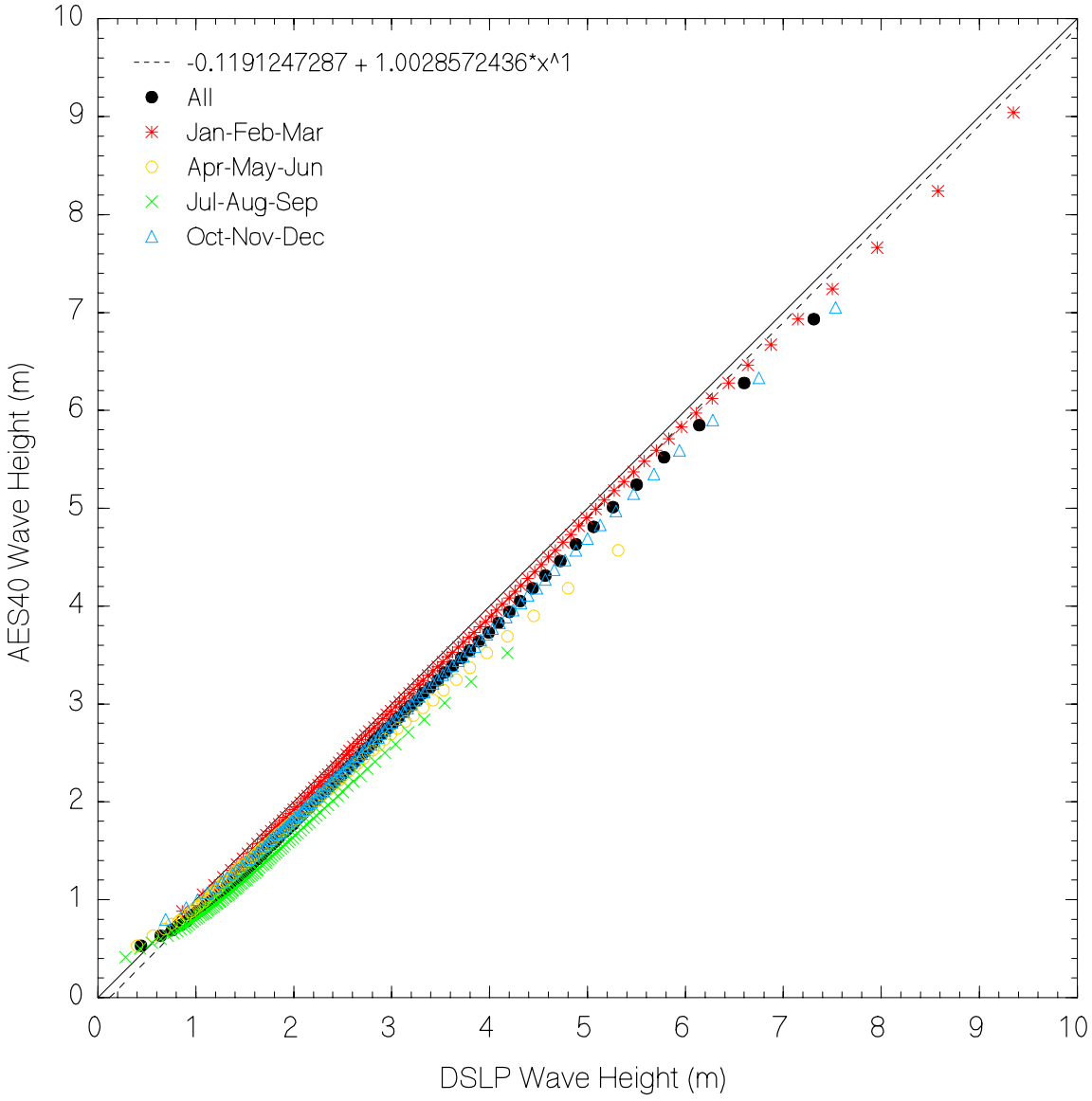

Figure 14 Quantile-quantile comparisons of DSLP (adjusted) and AES40 wave height (m) in 1990 by season

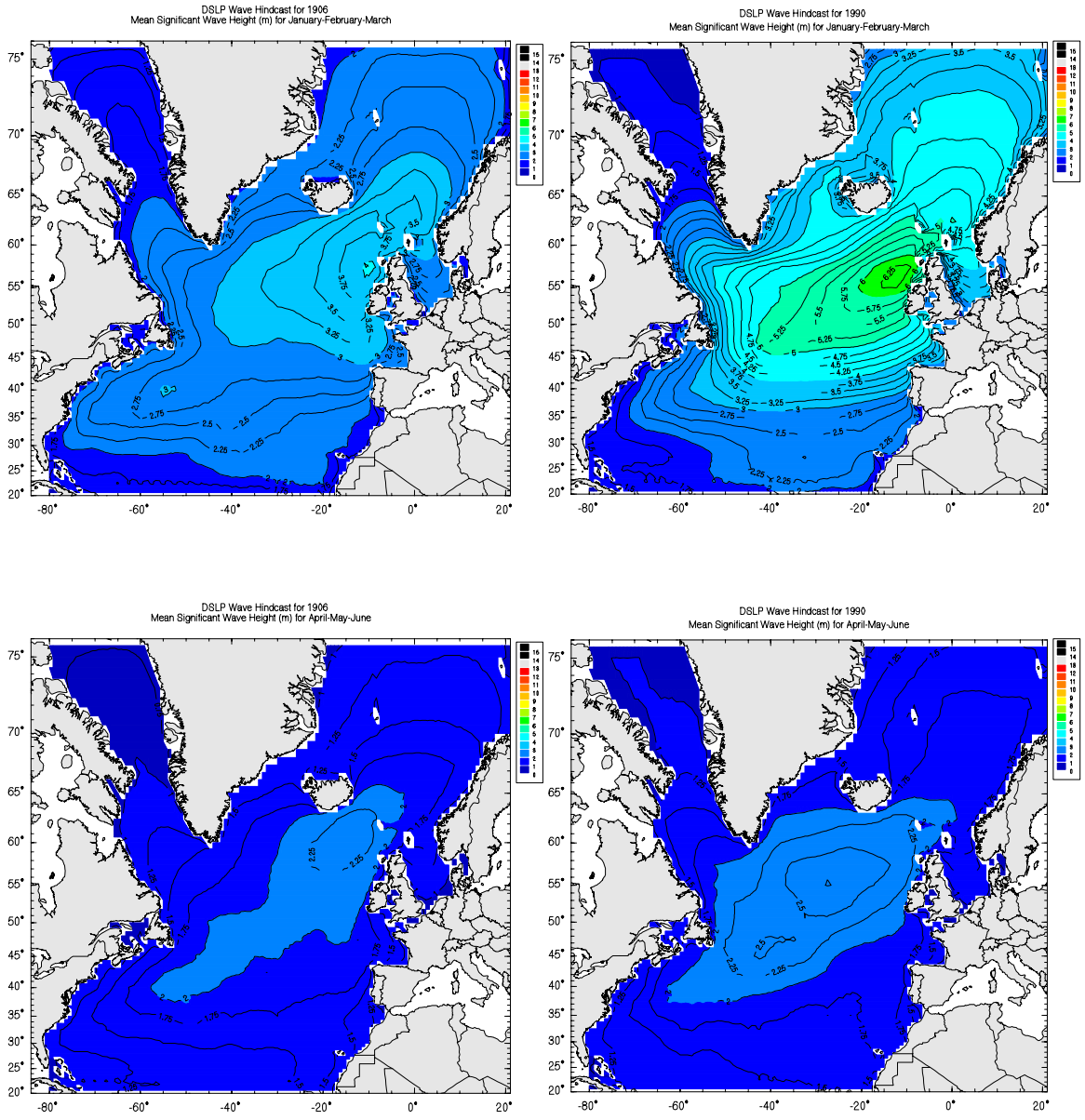

Figure 15 Dec-Jan-Feb (top) and Apr-May-Jun (bottom) mean significant wave height for 1906 (left) and 1990 (right)

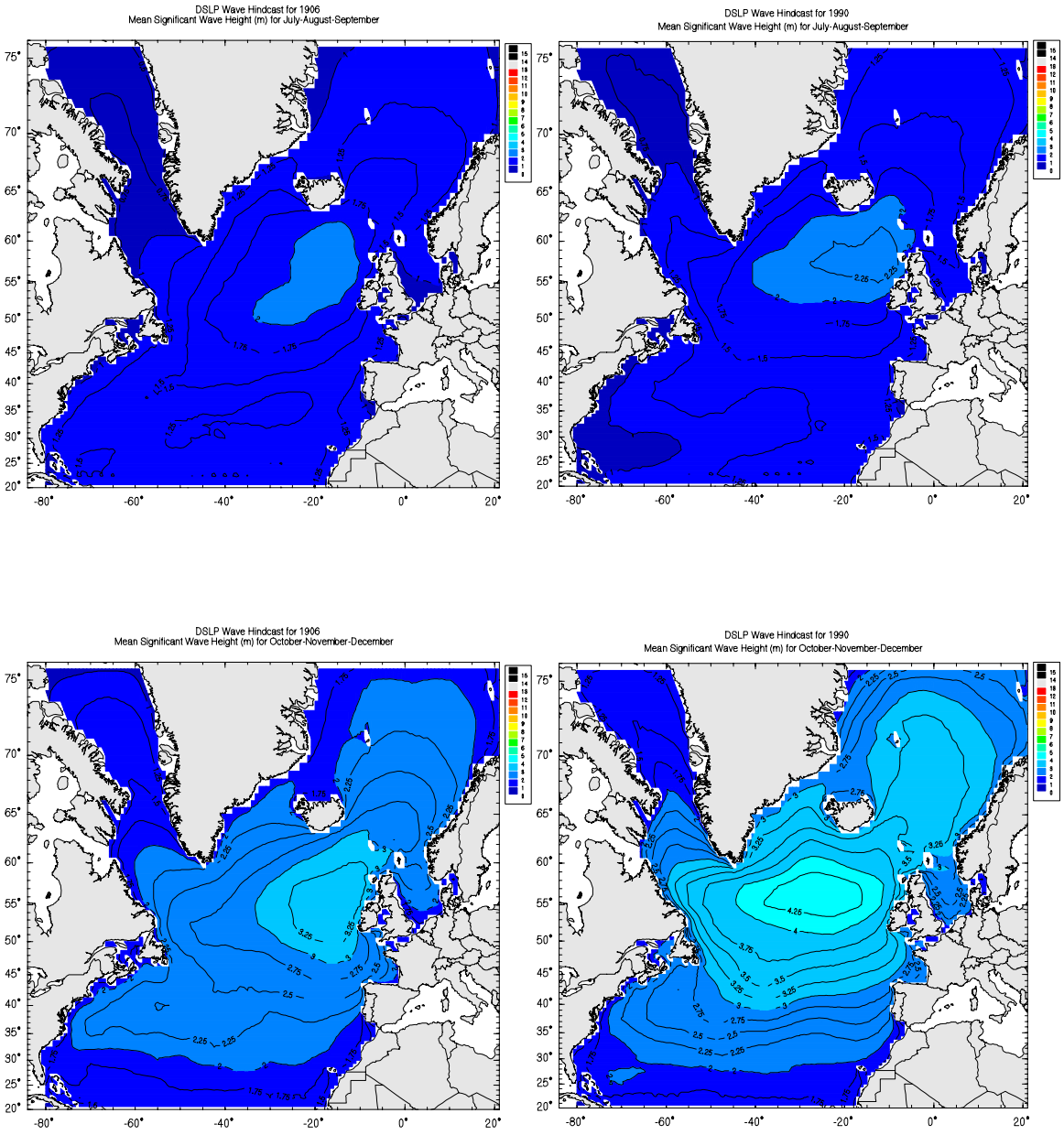

Figure 16 Jul-Aug-Sep (top) and Oct-Nov-Dec (bottom) mean significant wave height for 1906 (left) and 1990 (right)